Computational Mechanics 25 (2000) 157–168 © Springer-Verlag 2000

Meshless shape design sensitivity analysis and optimization for contact problem with friction

N. H. Kim, K. K. Choi, J. S. Chen, Y. H. Park

Abstract In this paper, a continuum-based shape design sensitivity formulation for a frictional contact problem with a rigid body is proposed using a meshless method. The contact condition is imposed using the penalty method that regularizes the solution of variational inequality. The shape dependency of the contact variational form with respect to the design velocity field is obtained. The dependency of the response with respect to the shape of the rigid body is also considered. It is shown that the sensitivity equation needs to be solved at the final converged load step for the frictionless contact problem, whereas for the frictional contact case the sensitivity solution is needed at the converged configuration of each load step because the sensitivity of the current load step depends on that of the previous load step. The continuum-based contact formulation and consistent linearization is critical for accurate shape design sensitivity results. The accuracy of the proposed method is compared with the finite difference result and excellent agreement is obtained for a door seal contact example. A design optimization problem is formulated and solved to reduce the contact gap opening successfully in a demonstration of the proposed method.

1 Introduction

The contact problem in linear elasticity can be categorized as a free boundary value problem. In general, the region where contact occurs is unknown until the solution is obtained. Stampacchia and Lions [1, 2], pioneers in this field, formulated the free boundary value problem as a variational inequality (VI). The VI in linear elasticity can be considered as the projection of a solution in Hilbert space into a convex subset. Since the projection is a type of constraint, VI can be reformulated as a constrained minimization problem. This problem can then be solved by either the Lagrange multiplier method or the penalty method. Hughes et al. [3], proposed a finite element analysis (FEA) method for the contact problem, with a small deformation assumption. Kikuchi and Oden [4] studied contact VI theoretically from an engineering standpoint and formulated it as a constrained minimization problem.

As the structure experiences large deformation, the small deformation assumption is no longer valid. New algorithms for general large deformation contact problems were proposed in several papers. For example, Wriggers and Simo [5] suggested an algorithm for fully nonlinear contact problems by introducing a contact tangent stiffness matrix. Parisch [6] proposed a three-dimensional contact algorithm and used a linear master segment for discretization of contact surface. Saleeb et al. [7] developed a contact algorithm for arbitrary curved geometry. Laursen and Simo [8] proposed a continuum-based contact algorithm. The contact condition is imposed on both the continuum and discrete domains. The continuum-based formulation is critical for the continuum-based shape design sensitivity analysis (DSA) method proposed in this paper.

Since the mechanism of frictional phenomena is quite complicated, a representative mathematical model of friction is critically important. The classical Coulomb friction law is simple and is commonly used in many applications. Oden and Martins [9] studied dynamic friction law extensively where frictional effects depend on the speed of relative slip and interface asperities. However in the usual range of engineering application, dynamic effects of friction are negligible [9]. Michalowski and Mroz [10] developed a friction model based on nonassociative elasto-plasticity, and Wriggers et al. [11] extended their model using a material interface law to describe frictional phenomena. They divided tangential slip into a micro-slip caused by elastic deformation of asperities and a macro-slip due to relative plastic sliding of asperities.

Considerable effort has also been devoted toward the development of DSA methods for linear contact problems. Mignot [12] proved mathematically that the projection on the convex set in the Hilbert space is directionally differentiable. Sokolowski and Zolesio [13] derived a sensitivity formulation for VI from Mignot's result. They concluded that the solution of VI is conically differentiable (or directionally differentiable) and its shape sensitivity is a solution of another VI, which is a projection onto a common convex set of tangential and orthogonal subspaces. Many researchers have also developed DSA methods for nonlinear contact problems. Spivey and Tortorelli [14] presented a sensitivity formulation of the nonlinear frictionless contact problem for beam, and optimized the geometry of the rigid surface. Antunez and

N. H. Kim (✉), K. K. Choi, J. S. Chen, Y. H. Park
Center for Computer-Aided Design
and Department of Mechanical Engineering,
The University of Iowa, Iowa City, IA 52242, USA

This research was supported by National Science Foundation (DMS 98-74015) and U.S. Army TACOM through the Automotive Research Center (DAAE07-94-C-R094).

Kleiber [15] derived a sensitivity formulation of the contact problem using an Eulerian approach to analyze the structure. Pollock and Noor [16] developed a nonlinear dynamic sensitivity formulation using the discrete DSA method by taking derivatives of the finite element matrix. All the aforementioned researches in the nonlinear contact sensitivity analysis are confined to non-shape design sensitivity formulations.

In this paper, a continuum-based DSA method for shape design variables is presented for the contact problem of nearly incompressible hyper-elastic material (rubber-type material). Since the contact formulation is independent of the constitutive model, the proposed method can be applied to other material models if appropriate structural sensitivity formulation is used. The shape of rubber components is crucial to the contact force characteristics and the total volume of elastomer. Under the regularity assumption, Santos and Choi [17] derived shape sensitivity of nonlinear elastic materials. This method was extended to the buckling load factor of nonlinear structures with elastic materials by Park and Choi [18]. Recently, Choi and Duan [19] formulated nonlinear shape sensitivity of hyper-elastic material using ABAQUS. When large loads are applied, however, a mesh distortion problem is encountered in the nonlinear sensitivity analysis of a 2-D engine mount example.

The computational difficulties associated with the nonlinear analysis of the hyper-elastic material are due to the complexities involved in very large deformation and incompressible constraints. An effective numerical method that can handle large deformation is highly desirable for analysis of rubber components. The meshless method is an ideal choice since, unlike the conventional FEA method, the solution is much less sensitivity to the mesh distortion. Lancaster and Slakauskas [20] introduced the idea of the moving least squares method to interpolate surfaces. Since then, several researchers applied a similar concept to structural problems. Belytschko et al. [21], proposed the Element Free Galerkin (EFG) method with an accurate numerical integration method and accurate treatment of essential boundary conditions. Liu et al. [22, 23] developed the Reproducing Kernel Particle Method (RKPM) by introducing a modified kernel function that is constructed based on the enforcement of reproducing conditions such that the kernel estimates of displacement variables exactly reproduce polynomials up to certain degree. The RKPM was further extended to highly nonlinear and contact problems by Chen et al. [24, 25, 26]

In this paper, RKPM is utilized for the analysis tool, and, thus, DSA. A continuum-based shape DSA formulation is developed for a large deformation problem, which has frictional contact with a rigid surface. A nearly incompressible hyper-elastic material model is solved using a pressure projection method [29].

2
Reproducing kernel particle method

Liu et al. [22, 23] developed RKPM by introducing a modified kernel function that is constructed based on the enforcement of reproducing conditions such that the kernel estimates of displacement variables exactly reproduce polynomials up to a certain order. In RKPM, a displacement function $z(x)$ is approximated using a reproducing kernel approximation as

$$z^{\mathrm{R}}(x) = \int_{\Omega} C(x; x-y)\, \phi_a(x-y)\, z(y)\mathrm{d}y \tag{1}$$

where $z^{\mathrm{R}}(x)$ is the reproduced displacement function of $z(x)$ and $\phi_a(x-y)$ is the kernel function (or weight function) with a support measure of "a". In Eq. (1), $C(x; x-y)$ is the correction function defined by

$$C(x; x-y) = \mathbf{q}(x)^{\mathrm{T}}\mathbf{H}(x-y) \tag{2}$$

where $\mathbf{H}(x)^{\mathrm{T}} = [1, x, x^2, \ldots, x^n]$ and $\mathbf{q}(x)^{\mathrm{T}} = [q_0(x), q_1(x), \ldots, q_n(x)]$ are the interpolation function and unknown coefficient vector, respectively. In Eq. (2), $\mathbf{q}(x)$ is determined by imposing the n-th order completeness requirement. Expanding $z(y)$ in Eq. (1) using Taylor series expansion and imposing the n-th order completeness condition yield

$$\begin{aligned} z^{\mathrm{R}}(x) &= \int_{\Omega} C(x; x-y)\, \phi_a(x-y)\, z(y)\mathrm{d}y \\ &= \bar{m}_0(x)z(x) + \sum_{n=1}^{\infty} \frac{(-1)^n}{n!}\bar{m}_n(x)\frac{\mathrm{d}^n z(x)}{\mathrm{d}x^n} \end{aligned} \tag{3}$$

where

$$\bar{m}_n(x) = \sum_{k=1}^{n} q_k(x) m_{n+k}(x) \tag{4}$$

$$m_n(x) = \int_{\Omega} (x-y)^n \phi_a(x-y)\mathrm{d}y \tag{5}$$

For the reproduced function to exactly represent original function up to n-th order which is used as the reproducing condition,the following conditions should be satisfied,

$$\bar{m}_0(x) = 1 \quad \bar{m}_k(x) = 0 \quad k = 1, \ldots, n \tag{6}$$

which means $z^{\mathrm{R}}(x)$ in Eq. (5) represents $z(x)$ exactly up to the n-th order derivative. Equation (6) represents the following set of equations (reproducing condition):

$$\mathbf{M}(x)\mathbf{q}(x) = \mathbf{H}(0) \tag{7}$$

$$\mathbf{M}(x) = \begin{bmatrix} m_0(x) & m_1(x) & \ldots & m_n(x) \\ m_1(x) & m_2(x) & \ldots & m_{n+1}(x) \\ \cdot & \cdot & \ldots & \cdot \\ m_n(x) & m_{n+1}(x) & \ldots & m_{2n}(x) \end{bmatrix} \tag{8}$$

$$\mathbf{H}(0)^{\mathrm{T}} = [1, 0, \ldots, 0] \tag{9}$$

Thus, the coefficient of reproducing condition $\mathbf{q}(x)$ can be obtained by solving Eq. (7). The correction function $C(x; x-y)$ can be computed from Eq. (2)

$$C(x; x-y) = \mathbf{H}(0)^{\mathrm{T}}\mathbf{M}(x)^{-1}\mathbf{H}(x-y) \tag{10}$$

Introducing Eq. (10) into Eq. (1) leads to the following Reproducing Kernel approximation:

$$z^{\mathrm{R}}(x) = \mathbf{H}(0)^{\mathrm{T}}\mathbf{M}(x)^{-1} \int_{\Omega} \mathbf{H}(x-y)\, \phi_a(x-y) z(y)\mathrm{d}y \tag{11}$$

To develop a shape function for discrete approximation, Eq. (11) must be discretized. Suppose that the domain Ω is discretized by a set of particles $[x_1, ..., x_{\mathrm{NP}}]$, where x_I is the location of particle I, and NP is the total number of particles. Using a simple trapezoidal rule, Eq. (11) is discretized into

$$z^{\mathrm{R}}(x) = \sum_{I=1}^{\mathrm{NP}} C(x; x - x_I)\, \phi_a(x - x_I) z_I \Delta x_I \tag{12}$$

where Δx_I is a measure of length associate with node I. It is hard to determine Δx_I in a multi-dimensional case but it can be treated as a weight of the nodal value. Since the purpose of discretizing the continuous reproducing equation is to obtain a set of shape functions, one can simply set Δx_I to unity in the discretization of Eq. (1) and applying the reproducing conditions on the discretized equation to yield Eq. (12) with $\Delta x_I = 1$. Note that the resulting moment matrix $\mathbf{M}(x)$ is also expressed in a discrete form with unit weight. Equation (12) can be rewritten, using generalized displacement d_I, as

$$z^{\mathrm{R}}(x) = \sum_{I=1}^{\mathrm{NP}} \Phi_I(x) d_I \tag{13}$$

where $\Phi_I(x) = C(x; x - x_I)\, \phi_a(x - x_I)$. The function $\Phi_I(x)$ is interpreted as the particle or meshless shape function of particle I, and d_I is the associated coefficient of approximation, often called the generalized displacement. The shape function $\Phi_I(x_J)$ depends on the global coordinate x_J, whereas the shape function of the finite element method depends on a coordinate of reference geometry. In large deformation problems, a Lagrangian shape function is proposed by Chen et al. [24] to assure kernel stability throughout the course of large material deformation and to reduce CPU time since the shape functions and their material derivatives are computed only at the undeformed stage. It should also be noted that, in general, the meshless shape function does not bear the Kronecker delta properties, i.e., $\Phi_I(x_J) \neq \delta_{IJ}$. Therefore, for a general function $z(x)$ which is not a polynomial, d_I in Eq. (13) is not the nodal value of $z(x)$.

To specify essential boundary conditions, i.e., prescribed value at node points, the Lagrange multiplier method can be used to impose those conditions. Let the potential of the structure be U. The total potential becomes

$$\Pi = U - \int_{\Gamma_D} \lambda_i (z_i - \zeta_i) \mathrm{d}\Gamma \tag{14}$$

where Γ_D is the essential boundary and $\boldsymbol{\zeta}$ is the prescribed displacement vector. A summation rule is used for the repeated right subscript. The variation of this total potential is

$$\bar{\Pi} = \bar{U} - \int_{\Gamma_D} \lambda_i \bar{z}_i \,\mathrm{d}\Gamma - \int_{\Gamma_D} \bar{\lambda}_i (z_i - \zeta_i) \mathrm{d}\Gamma \tag{15}$$

where $\bar{\mathbf{z}}$ means variation of displacement. The "over bar" is used to denote the first-order variation throughout this paper since the usual notation of the variation δ can be confused with design perturbation or Dirac delta function. Also, $\mathbf{z}$ denotes the displacement function instead of usual notation $\mathbf{u}$, which is reserved as the design parameter. If the problem contains many boundary conditions then the excessive number of the Lagrange multiplier greatly increases the size of the system matrix. The semi-positive definiteness of the system matrix also needs special treatment in the solution phase. For the case of the contact problem, since contact constraints are imposed through the physical coordinate of the material point, it is inconvenient or impossible to use the generalized displacement. In this work, a direct transformation method proposed by Chen et al. [24] to treat boundary conditions and contact constraints systematically is employed.

3
Frictional contact analysis

The contact conditions can be divided into the normal impenetration and tangential slip. The normal impenetration condition prevents penetration of one body into another and the tangential slip represents frictional behavior of a contact surface. When there exists a friction in the contact problem, the solution depends on the history of the load applied to the structure. Classical Coulomb friction law is commonly used in computational mechanics. As an alternative to Coulomb frictional law, a frictional interface law by Wriggers et al. [11] is utilized in this paper. This friction law is a regularized version of Coulomb law where the regularization parameter can be related to experimental observation.

3.1
Contact condition with rigid surface

Figure 1 shows a general contact condition with a rigid surface in R^2. Since the motion of the rigid surface is prescribed throughout the analysis, a natural coordinate ξ is used to represent the location on the rigid surface. The coordinate of contact point $\mathbf{x}_c$ can be represented using a natural coordinate at the contact point ξ_c by

$$\mathbf{x}_c = \mathbf{x}_c(\xi_c) \tag{16}$$

The normal impenetration condition can be imposed on the structure by measuring the distance between a part of the structural boundary Γ_c and the surface of the rigid surface as shown in Fig. 1. The normal impenetration

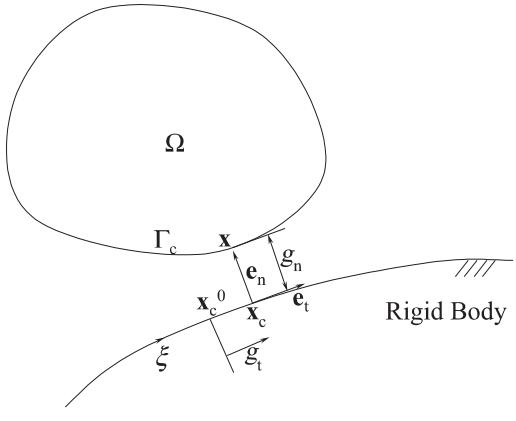

Fig. 1. Frictional contact condition in R^2

condition can be defined, using the normal gap function g_n which measures the normal distance, as

$$g_n \equiv (\mathbf{x} - \mathbf{x}_c(\xi_c))^T \mathbf{e}_n(\xi_c) \geq 0, \quad \mathbf{x} \in \Gamma_c \tag{17}$$

where $\mathbf{e}_n(\xi_c)$ is the unit outward normal vector of the rigid surface at the contact point. The contact point $\mathbf{x}_c$ that corresponds to the body point $\mathbf{x} \in \Gamma_c$ is determined by solving the following nonlinear equation,

$$\varphi(\xi_c) = (\mathbf{x} - \mathbf{x}_c(\xi_c))^T \mathbf{e}_t(\xi_c) = 0 \tag{18}$$

where $\mathbf{e}_t = \mathbf{t}/\|\mathbf{t}\|$ is the unit tangential vector and $\mathbf{t} = \mathbf{x}_{c,\xi}$ is the tangential vector at the contact point. Equation (18) is called a contact consistency condition. In Eq. (18) $\mathbf{x}_c(\xi_c)$ is the closest projection point of $\mathbf{x} \in \Gamma_c$ onto the rigid surface by imposing the contact consistency condition.

As the contact point moves along the rigid surface, there exists a frictional force along the tangential direction of the rigid surface, that resists the tangential relative movement. Tangential slip function g_t is the measure of the relative movement of the contact point along the rigid surface,

$$g_t \equiv \|\mathbf{t}^0\|(\xi_c - \xi_c^0) \tag{19}$$

where $\mathbf{t}^0$ and ξ_c^0 are the tangential vector and natural coordinate of the previous converged time step or load step. Right super-script 0 denotes the previous configuration time.

It is well known that the contact problem is classified as a VI problem. Since a VI problem is equivalent to a constrained minimization problem, the original VI problem can be converted to a constrained minimization problem, which can be solved using an approximation method, e.g., the penalty method. If there exists a region Γ_c which violates the normal impenetration condition of Eq. (17), it is penalized using a penalty function. Similarly, the tangential movement of Eq. (19) can also be penalized under stick condition. Define the contact penalty function for the penetrated region by

$$P = \frac{1}{2}\omega_n \int_{\Gamma_c} g_n^2 \, d\Gamma + \frac{1}{2}\omega_t \int_{\Gamma_c} g_t^2 \, d\Gamma \tag{20}$$

where ω_n and ω_t are penalty parameters for normal impenetration and tangential slip. The penalty function defined in Eq. (20) leads to an exterior penalty method where the solution approaches from the infeasible region. This means the normal impenetration condition will be violated, but the amount of the violation is decreased as the penalty parameter is increased.

The first variation of P yields the contact variational form, which is defined by

$$b(\mathbf{z}, \bar{\mathbf{z}}) \equiv \omega_n \int_{\Gamma_c} g_n \bar{g}_n \, d\Gamma + \omega_t \int_{\Gamma_c} g_t \bar{g}_t \, d\Gamma \tag{21}$$

In Eq. (21), $\omega_n g_n$ corresponds to the compressive normal force and $\omega_t g_t$ corresponds to the tangential traction force. The tangential traction force increases linearly with tangential slip g_t until it reaches a normal force multiplied by the friction coefficient. The contact variational form Eq. (21) can be expressed in terms of the displacement variation. For the convenience of the derivations to follow, define several scalar symbols

$$\begin{aligned} &\alpha \equiv \mathbf{e}_n^T \mathbf{x}_{c,\xi\xi}, \quad \beta \equiv \mathbf{e}_t^T \mathbf{x}_{c,\xi\xi}, \quad \gamma \equiv \mathbf{e}_n^T \mathbf{x}_{c,\xi\xi\xi}, \\ &c \equiv \|\mathbf{t}\|^2 - g_n \alpha, \quad v \equiv \|\mathbf{t}\|\|\mathbf{t}^0\|/c \end{aligned} \tag{22}$$

Note that if the rigid surface is approximated by a piecewise linear function, then $\alpha = \beta = \gamma = 0$ and $v = 1$.

By taking the first variation of the normal gap function in Eq. (17) and using the variation of the contact consistency condition in Eq. (18), the first variation of the normal gap function can be obtained as

$$\bar{g}_n(\mathbf{z}; \bar{\mathbf{z}}) = \bar{\mathbf{z}}^T \mathbf{e}_n \tag{23}$$

where the variation of the natural coordinate at the contact point is canceled by an orthogonal condition. The normal gap function can vary only in a normal direction of the rigid surface, which is physically meaningful. The first variations of the unit tangential and normal vector can also be obtained as

$$\bar{\mathbf{e}}_t = \frac{\alpha}{c}\mathbf{e}_n(\bar{\mathbf{z}}^T \mathbf{e}_t) \tag{24}$$

$$\bar{\mathbf{e}}_n = -\frac{\alpha}{c}\mathbf{e}_t(\bar{\mathbf{z}}^T \mathbf{e}_t) \tag{25}$$

The first variation of the tangential slip function, Eq. (19), becomes,

$$\bar{g}_t = \|\mathbf{t}^0\|\bar{\xi}_c = v\bar{\mathbf{z}}^T \mathbf{e}_t \tag{26}$$

Note that the first variations of $\|\mathbf{t}^0\|$ and ξ_c^0 are zero since they are the solutions of the previous time step (or load step) that are fixed at the current load step. By using Eqs. (23) and (26) the contact variational form Eq. (21) can be rewritten in terms of the variation of displacement as

$$b(\mathbf{z}, \bar{\mathbf{z}}) = \omega_n \int_{\Gamma_c} g_n \bar{\mathbf{z}}^T \mathbf{e}_n \, d\Gamma + \omega_t \int_{\Gamma_c} v g_t \bar{\mathbf{z}}^T \mathbf{e}_t \, d\Gamma \tag{27}$$

The first term comes from the normal impenetration condition and the magnitude of the normal impenetration force is proportional to the violation of the impenetration condition. The second term comes from frictional effects. The frictional traction force acts in the tangential direction proportional to the tangential slip and is scaled by curvature through v. The frictional force is bounded above by a compressive normal force multiplied by the friction coefficient in Coulomb friction law. But for the case of small slip (micro-displacement), the traction force is proportional to the tangential slip. The penalty parameter ω_t is a constant for this case. Figure 2 shows the friction curve used in this paper. An exact stick condition represented by a step function in the classical Coulomb friction

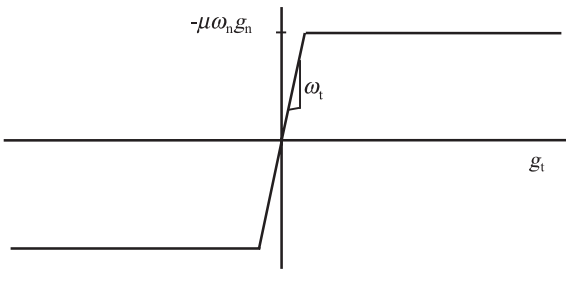

Fig. 2. Frictional interface model

law is now regularized by a piecewise linear function as shown in Fig. 2 with the penalty parameter ω_t serving as a regularization parameter. As demonstrated in Fig. 2, this regularized friction law reduces to the classical law as $\omega_t \to \infty$. A regularized stick condition occurs when:

$$|\omega_t g_t| \le |\mu \omega_n g_n| \tag{28}$$

Otherwise, it becomes a slip condition and $\omega_t g_t = -\mu \omega_n g_n$. In Eq. (28), μ is the Coulomb friction coefficient. For the case of the slip condition, the contact variational form must be modified. Thus Eq. (27) must be divided into two cases as

$$b(\mathbf{z}, \bar{\mathbf{z}}) = \omega_n \int_{\Gamma_c} g_n \bar{\mathbf{z}}^T \mathbf{e}_n \, d\Gamma + \begin{cases} +\omega_t \int_{\Gamma_c} v g_t \bar{\mathbf{z}}^T \mathbf{e}_t \, d\Gamma, & \text{if } |\omega_t g_t| \le |\mu \omega_n g_n| \\ -\mu \omega_n \operatorname{sgn}(g_t) \int_{\Gamma_c} v g_n \bar{\mathbf{z}}^T \mathbf{e}_t \, d\Gamma, & \text{otherwise} \end{cases} \tag{29}$$

3.2 Linearization of stick condition

As the structure experiences a finite deformation, the relation between the displacement and response becomes nonlinear. The contact constraints make the problem even more nonlinear. The Newton type method is the most popular tool to solve the nonlinear systems of equations in computational mechanics. Assume that the configuration of a structure at load step n is known. The configuration of structure at load step $n+1$ is computed using incremental analysis, which is formulated by a linearization procedure. The contact variational form for the stick condition at load step $n+1$ can be written as

$$\begin{aligned} b({}^{n+1}\mathbf{z}, \bar{\mathbf{z}}) &= \omega_n \int_{\Gamma_c} {}^{n+1}g_n \bar{\mathbf{z}}^{T\,n+1} \mathbf{e}_n \, d\Gamma \\ &\quad + \omega_t \int_{\Gamma_c} {}^{n+1}v^{n+1} g_t \bar{\mathbf{z}}^{T\,n+1} \mathbf{e}_t \, d\Gamma \\ &\equiv b_N({}^{n+1}\mathbf{z}, \bar{\mathbf{z}}) + b_T({}^{n+1}\mathbf{z}, \bar{\mathbf{z}}) \end{aligned} \tag{30}$$

where $b_N({}^{n+1}\mathbf{z}, \bar{\mathbf{z}})$ is the normal impenetration form and $b_T({}^{n+1}\mathbf{z}, \bar{\mathbf{z}})$ is the tangential stick form. The left superscript is used to denote the configuration time and will be omitted unless necessary for clarification. Equation (30) is linearized at load step $n+1$ using the incremental form. The incremental form of the normal gap and the tangential slip function can be computed using similar procedures for computing the first variations in Eqs. (23) and (26) as

$$\Delta g_n(\mathbf{z}; \Delta \mathbf{z}) = \mathbf{e}_n^T \Delta \mathbf{z} \tag{31}$$

$$\Delta g_t(\mathbf{z}; \Delta \mathbf{z}) = v \mathbf{e}_t^T \Delta \mathbf{z} \tag{32}$$

where $\Delta \mathbf{z}$ is an incremental displacement vector. The incremental form of unit normal and tangential vectors can be derived using similar procedure as in Eqs. (24) and (25) as

$$\Delta \mathbf{e}_t = \frac{\alpha}{c} \mathbf{e}_n (\mathbf{e}_t^T \Delta \mathbf{z}) \tag{33}$$

$$\Delta \mathbf{e}_n = -\frac{\alpha}{c} \mathbf{e}_t (\mathbf{e}_t^T \Delta \mathbf{z}) \tag{34}$$

The standard linearization of a normal impenetration form in Eq. (30) leads to a normal impenetration bilinear form defined by

$$\begin{aligned} b_N^*(\mathbf{z}; \Delta \mathbf{z}, \bar{\mathbf{z}}) &= \omega_n \int_{\Gamma_c} \bar{\mathbf{z}}^T \mathbf{e}_n \mathbf{e}_n^T \Delta \mathbf{z} \, d\Gamma \\ &\quad - \omega_n \int_{\Gamma_c} (\alpha g_n / c) \bar{\mathbf{z}}^T \mathbf{e}_t \mathbf{e}_t^T \Delta \mathbf{z} \, d\Gamma \end{aligned} \tag{35}$$

Note that, in Eq. (35), there is a component in the tangential direction because of the curvature effects. The linearization of a tangential stick condition leads to the tangential stick bilinear form defined by

$$\begin{aligned} b_T^*(\mathbf{z}; \Delta \mathbf{z}, \bar{\mathbf{z}}) &= \omega_t \int_{\Gamma_c} v^2 \bar{\mathbf{z}}^T \mathbf{e}_t \mathbf{e}_t^T \Delta \mathbf{z} \, d\Gamma + \omega_t \int_{\Gamma_c} (\alpha v g_t / c) \bar{\mathbf{z}}^T \\ &\quad \times (\mathbf{e}_n \mathbf{e}_t^T + \mathbf{e}_t \mathbf{e}_n^T) \Delta \mathbf{z} \, d\Gamma + \omega_t \int_{\Gamma_c} (v g_t / c^2) \\ &\quad \times ((\gamma \|\mathbf{t}\| - 2\alpha\beta) g_n - \beta \|\mathbf{t}\|^2) \bar{\mathbf{z}}^T \mathbf{e}_t \mathbf{e}_t^T \Delta \mathbf{z} \, d\Gamma \end{aligned} \tag{36}$$

In Eqs. (35) and (36) higher-order terms are ignored. The contact bilinear form is the sum of Eqs. (35) and (36),

$$b^*(\mathbf{z}; \Delta \mathbf{z}, \bar{\mathbf{z}}) = b_N^*(\mathbf{z}; \Delta \mathbf{z}, \bar{\mathbf{z}}) + b_T^*(\mathbf{z}; \Delta \mathbf{z}, \bar{\mathbf{z}}) \tag{37}$$

For the case of the stick condition, the contact bilinear form Eq. (37) is symmetric with respect to the incremental displacement and the variation of displacement. This is expected since the elastic stick contact condition is a conservative system.

3.3 Linearization of slip condition

As the contact point is forced to move along the contact surface leading to a violation of Eq. (28), the slip contact condition is applied and the second equation of Eq. (29) is used. Contact variational form for slip condition at load step $n+1$ is

$$\begin{aligned} b({}^{n+1}\mathbf{z}, \bar{\mathbf{z}}) &= \omega_n \int_{\Gamma_c} {}^{n+1}g_n \bar{\mathbf{z}}^{T\,n+1} \mathbf{e}_n \, d\Gamma - \mu \omega_n \operatorname{sgn}({}^{n+1}g_t) \\ &\quad \times \int_{\Gamma_c} {}^{n+1}v^{n+1} g_n \bar{\mathbf{z}}^{T\,n+1} \mathbf{e}_t \, d\Gamma \end{aligned} \tag{38}$$

The first term is the same as the contact variational form for a stick condition and its normal impenetration bilinear form $b_N^*(\mathbf{z}; \Delta \mathbf{z}, \bar{\mathbf{z}})$ is given in Eq. (35). For the case of the slip contact condition, the tangential penalty parameter ω_t is related to normal impenetration penalty parameter ω_n according to relation

$$\omega_t = -\mu \omega_n \operatorname{sgn}(g_t) \tag{39}$$

The tangential slip form for the slip condition is

$$b_T({}^{n+1}\mathbf{z}, \bar{\mathbf{z}}) = \omega_t \int_{\Gamma_c} {}^{n+1}v^{n+1} g_n \bar{\mathbf{z}}^{T\,n+1} \mathbf{e}_t \, d\Gamma \tag{40}$$

The linearization of Eq. (40) leads to a tangential slip bilinear form as

$$b_{\mathrm{T}}^{*}(\mathbf{z};\Delta\mathbf{z},\bar{\mathbf{z}}) = \omega_{\mathrm{t}}\int_{\Gamma_{\mathrm{c}}} v\bar{\mathbf{z}}^{\mathrm{T}}\mathbf{e}_{\mathrm{t}}\mathbf{e}_{\mathrm{n}}^{\mathrm{T}}\Delta\mathbf{z}\,\mathrm{d}\Gamma + \omega_{\mathrm{t}}\int_{\Gamma_{\mathrm{c}}}(\alpha v g_{\mathrm{n}}/c)\bar{\mathbf{z}}^{\mathrm{T}} \times(\mathbf{e}_{\mathrm{n}}\mathbf{e}_{\mathrm{t}}^{\mathrm{T}} + \mathbf{e}_{\mathrm{t}}\mathbf{e}_{\mathrm{n}}^{\mathrm{T}})\Delta\mathbf{z}\,\mathrm{d}\Gamma + \omega_{t}\int_{\Gamma_{\mathrm{c}}}(v g_{\mathrm{n}}/c^{2}) \times((\gamma\|\mathbf{t}\| - 2\alpha\beta)g_{\mathrm{n}} - \beta\|\mathbf{t}\|^{2})\bar{\mathbf{z}}^{\mathrm{T}}\mathbf{e}_{\mathrm{t}}\mathbf{e}_{\mathrm{t}}^{\mathrm{T}}\Delta\mathbf{z}\,\mathrm{d}\Gamma \tag{41}$$

The contact bilinear form is the sum of Eqs. (35) and (41) as

$$b^{*}(\mathbf{z};\Delta\mathbf{z},\bar{\mathbf{z}}) = b_{\mathrm{N}}^{*}(\mathbf{z};\Delta\mathbf{z},\bar{\mathbf{z}}) + b_{\mathrm{T}}^{*}(\mathbf{z};\Delta\mathbf{z},\bar{\mathbf{z}}) \tag{42}$$

For the case of the slip condition, the contact bilinear form Eq. (42) is not symmetric with respect to the incremental displacement and the variation of the displacement. The system is no longer conservative as the frictional slipping dissipates energy.

3.4 Variational principle for finite deformation with frictional contact problem

Even though the contact formulation derived is applicable for general contact problems, it is applied to hyper-elastic material in this paper. For nearly incompressible hyper-elastic material, there exists a strain energy density function, and the stress-strain relation can be established using the derivative of a strain energy density function. The nearly incompressibility constraint can be formulated using a perturbed Lagrangian formulation [30] or a penalty method in conjunction with a pressure projection [29, 32] as a generalization of the perturbed Lagrangian formulation. The Rivlin-type material model with nearly incompressible constraint is used in this paper. For the case of hyper-elastic material with a frictional contact problem, the variational principle for virtual work can be written as

$$a({}^{n+1}\mathbf{z},\bar{\mathbf{z}}) + b({}^{n+1}\mathbf{z},\bar{\mathbf{z}}) = \ell(\bar{\mathbf{z}}), \quad \forall\,\bar{\mathbf{z}} \in Z \tag{43}$$

where $a({}^{n+1}\mathbf{z},\bar{\mathbf{z}})$ is the variational form for the structural part, $\ell(\bar{\mathbf{z}})$ is a work done by an external force through variational displacement, and Z is the space of kinematically admissible virtual displacements. The variational form and linearized form for structure are provided in Refs. [24, 31] and a pressure projection method is employed following Ref. [32]. Let the current load step be $n+1$ and let the current iteration count be $k+1$. Assuming that the external force is independent of displacement, the linearized incremental equation of Eq. (43) is obtained as

$$a^{*}({}^{n+1}\mathbf{z}^{k};\Delta\mathbf{z}^{k+1},\bar{\mathbf{z}}) + b^{*}({}^{n+1}\mathbf{z}^{k};\Delta\mathbf{z}^{k+1},\bar{\mathbf{z}}) = \ell(\bar{\mathbf{z}}) - a({}^{n+1}\mathbf{z}^{k},\bar{\mathbf{z}}) - b({}^{n+1}\mathbf{z}^{k},\bar{\mathbf{z}}), \quad \forall\,\bar{\mathbf{z}} \in Z \tag{44}$$

Equation (44) is linear in incremental displacement for a given displacement variation. The linearized system of Eq. (44) is solved iteratively with respect to incremental displacement until the residual forces (right side of Eq. (44)) vanish at each load step. The path dependency of the problem comes from the tangential slip function.

4 Design sensitivity formulation for frictional contact problem

A structural system in the equilibrium configuration at load step n corresponding to the initial design ${}^{0}\Omega$ is given in Eq. (43). Let the design be perturbed by parameter τ and the perturbed design has an equilibrium configuration

$$a_{0_{\Omega_\tau}}(\mathbf{z}_\tau,\bar{\mathbf{z}}_\tau) + b_{0_{\Gamma_\tau}}(\mathbf{z}_\tau,\bar{\mathbf{z}}_\tau) = \ell_{0_{\Omega_\tau}}(\bar{\mathbf{z}}_\tau), \quad \forall\,\bar{\mathbf{z}}_\tau \in Z_\tau \tag{45}$$

where the subscript ${}^{0}\Omega$ and ${}^{0}\Gamma$ indicate the dependence of these terms on the shape of the original configuration. Even though the solution of VI is directionally differentiable, the solution $\mathbf{z}_\tau(\mathbf{X}_\tau)$ of Eq. (45) referred to the initial coordinates $\mathbf{X}_\tau$ of the perturbed domain is assumed to be differentiable with respect to the shape design variable because of the regularization property of the penalty method. The material derivatives of the structural variational form and external load form in Eq. (45) for elastic or hyper-elastic material become

$$\frac{\mathrm{d}}{\mathrm{d}\tau}\left[a_{0_{\Omega_\tau}}(\mathbf{z}_\tau,\bar{\mathbf{z}}_\tau)\right]_{\tau=0} = a^{*}(\mathbf{z};\dot{\mathbf{z}},\bar{\mathbf{z}}) + a'_{\mathrm{V}}(\mathbf{z},\bar{\mathbf{z}}) \tag{46}$$

$$\frac{\mathrm{d}}{\mathrm{d}\tau}\left[\ell_{0_{\Omega_\tau}}(\bar{\mathbf{z}}_\tau)\right]_{\tau=0} = \ell'_{\mathrm{V}}(\bar{\mathbf{z}}) \tag{47}$$

where $\dot{\mathbf{z}}$ denotes the material derivative of the displacement function. For detailed derivations refer to Ref. [33]. The material derivative formulas for linear elastic material are discussed by Haug et al. [33], and Santos and Choi [17] for nonlinear elasticity.

4.1 Design sensitivity formulation for frictional contact

Before taking the first-order variation of the normal impenetration variational form, consider first the fundamental properties of differentiation related to the contact. The material derivative of structural point $\mathbf{x} \in \Omega$ at load step n is

$$\frac{\mathrm{d}}{\mathrm{d}\tau}(\mathbf{x}_\tau)|_{\tau=0} \equiv \frac{\mathrm{d}}{\mathrm{d}\tau}(\mathbf{X}_\tau + \mathbf{z}_\tau)|_{\tau=0} = \mathbf{V}(\mathbf{X}) + \dot{\mathbf{z}}(\mathbf{X}) \tag{48}$$

where $\mathbf{V}(\mathbf{X})$ is design velocity vector at $\mathbf{X}$ and the relation $\mathbf{x} = \mathbf{X} + \mathbf{z}$ is used. The configuration at ${}^{0}\Omega$ is perturbed in the direction of $\mathbf{V}(\mathbf{X})$ and the perturbation of configuration at load step n is affected by $\mathbf{V}(\mathbf{X})$ explicitly and $\dot{\mathbf{z}}(\mathbf{X})$ implicitly. On the other hand, the contact point on the master surface $\mathbf{X}_{\mathrm{c}} \in \Gamma_{\mathrm{c}}$ can be perturbed by the change of the natural coordinate corresponding to the contact point in the tangential direction as

$$\frac{\mathrm{d}}{\mathrm{d}\tau}(\mathbf{x}_{\mathrm{c}})|_{\tau=0} = \mathbf{V}_{\mathrm{c}}(\mathbf{X}_{\mathrm{c}}) + \mathbf{t}\frac{\mathrm{d}}{\mathrm{d}\tau}(\xi_{\mathrm{c}}) \tag{49}$$

where $\mathbf{V}_{\mathrm{c}}(\mathbf{X}_{\mathrm{c}})$ is the design velocity of the rigid surface at the contact point. The design perturbation of the rigid body can also be considered using Eq. (49).

Since the normal impenetration form appears in both the stick and slip conditions, the material derivative of the normal impenetration form is considered first. A normal impenetration form at the perturbed domain is

$$b_{N_\tau}(\mathbf{z}_\tau, \bar{\mathbf{z}}_\tau) = \omega_n \int_{\Gamma_{c_\tau}} g_{n_\tau} \mathbf{e}_{n_\tau}^T \bar{\mathbf{z}}_\tau \, d\Gamma_\tau \tag{50}$$

The derivative of normal impenetration form, Eq. (50), at the perturbed boundary Γ_τ is

$$\frac{d}{d\tau}[b_{N_\tau}(\mathbf{z}_\tau, \bar{\mathbf{z}}_\tau)]_{\tau=0} = \omega_n \int_{\Gamma_c} \left[\frac{d}{d\tau}(g_n)\mathbf{e}_n^T \bar{\mathbf{z}} + g_n \frac{d}{d\tau}(\mathbf{e}_n)^T \bar{\mathbf{z}} \right] d\Gamma + \omega_n \int_{\Gamma_c} \kappa g_n \mathbf{e}_n^T \bar{\mathbf{z}} (\mathbf{V}^T \mathbf{n}) d\Gamma \tag{51}$$

where κ is a curvature of the contact boundary and $\mathbf{V}$ is the design velocity field. The derivatives of the unit normal vector and the normal gap function depend on the derivative of the natural coordinate at the contact point, which can be obtained from the variation of the contact consistency condition Eq. (18) as

$$\frac{d}{d\tau}(\xi_c)|_{\tau=0} = (\|\mathbf{t}\|/c)(\mathbf{V} - \mathbf{V}_c + \dot{\mathbf{z}})^T \mathbf{e}_t + (g_n/c)\mathbf{V}_{c,\xi}^T \mathbf{e}_n \tag{52}$$

The material derivatives of the unit normal vector and the tangential vector can be expressed in terms of the design velocity and the material derivative of the displacement as

$$\frac{d}{d\tau}(\mathbf{e}_t)|_{\tau=0} = \frac{\alpha}{c}\left[(\mathbf{V} - \mathbf{V}_c + \dot{\mathbf{z}})^T \mathbf{e}_t + \frac{g_n}{c} \mathbf{V}_{c,\xi}^T \mathbf{e}_n \right] \mathbf{e}_n \tag{53}$$

$$\frac{d}{d\tau}(\mathbf{e}_n)|_{\tau=0} = -\frac{\alpha}{c}\left[(\mathbf{V} - \mathbf{V}_c + \dot{\mathbf{z}})^T \mathbf{e}_t + \frac{g_n}{c} \mathbf{V}_{c,\xi}^T \mathbf{e}_n \right] \mathbf{e}_t \tag{54}$$

For the case of a general rigid surface, the unit normal vector $\mathbf{e}_n$ and the tangential vector $\mathbf{e}_t$ may change as the shape changes. It is necessary to evaluate the derivative of the unit normal and tangential vectors of the rigid surface from Eqs. (53) and (54).

The material derivative of normal gap function can be found by taking variation of Eq. (17) as

$$\frac{d}{d\tau}(g_{n_\tau})|_{\tau=0} = \frac{d}{d\tau}\left[(\mathbf{x}_\tau - \mathbf{x}_{c_\tau})^T \mathbf{e}_{n_\tau} \right]_{\tau=0} = (\mathbf{V} - \mathbf{V}_c + \dot{\mathbf{z}})^T \mathbf{e}_n \tag{55}$$

Equation (55) implies that, for arbitrary perturbation of the structural shape, only the normal components of the perturbation contribute to the material derivative of the normal gap function. The material derivative of the normal impenetration form, Eq. (51), becomes

$$\frac{d}{d\tau}[b_{N_\tau}(\mathbf{z}_\tau, \bar{\mathbf{z}}_\tau)]_{\tau=0} = \omega_n \int_{\Gamma_c} \bar{\mathbf{z}}^T \mathbf{e}_n \mathbf{e}_n^T (\mathbf{V} - \mathbf{V}_c + \dot{\mathbf{z}}) d\Gamma - \omega_n \int_{\Gamma_c} (\alpha g_n/c) \bar{\mathbf{z}}^T \mathbf{e}_t \mathbf{e}_t^T (\mathbf{V} - \mathbf{V}_c + \dot{\mathbf{z}}) d\Gamma - \omega_n \int_{\Gamma_c} (g_n \|\mathbf{t}\|/c) \bar{\mathbf{z}}^r \mathbf{e}_t \mathbf{e}_n^T \mathbf{V}_{c,\xi} \, d\Gamma + \omega_n \int_{\Gamma_c} \kappa g_n \mathbf{e}_n^T \bar{\mathbf{z}} (\mathbf{V}^T \mathbf{n}) d\Gamma \tag{56}$$

Collecting the terms which have explicit dependence on the design velocity field from Eq. (56) and defining them as the normal impenetration fictitious load form,

$$b'_N(\mathbf{z}, \bar{\mathbf{z}}) = \omega_n \int_{\Gamma_c} \bar{\mathbf{z}}^T \mathbf{e}_n \mathbf{e}_n^T (\mathbf{V} - \mathbf{V}_c) d\Gamma - \omega_n \int_{\Gamma_c} (\alpha g_n/c) \bar{\mathbf{z}}^T \mathbf{e}_t \mathbf{e}_t^T (\mathbf{V} - \mathbf{V}_c) d\Gamma - \omega_n \int_{\Gamma_c} (g_n \|\mathbf{t}\|/c) \bar{\mathbf{z}}^T \mathbf{e}_t \mathbf{e}_n^T \mathbf{V}_{c,\xi} \, d\Gamma + \omega_n \int_{\Gamma_c} \kappa g_n \mathbf{e}_n^T \bar{\mathbf{z}} (\mathbf{V}^T \mathbf{n}) d\Gamma \tag{57}$$

The other two terms in the right side of Eq. (56) are of the same form as the normal impenetration bilinear form in Eq. (35). If the material derivative of the displacement is substituted into the incremental displacement, Eq. (56) becomes

$$\frac{d}{d\tau}[b_{N\tau}(\mathbf{z}_\tau, \bar{\mathbf{z}}_\tau)]_{\tau=0} = b_N^*(\mathbf{z}; \dot{\mathbf{z}}, \bar{\mathbf{z}}) + b'_N(\mathbf{z}, \bar{\mathbf{z}}) \tag{58}$$

The tangential slip function in Eq. (19) can be expressed at the perturbed domain as

$$g_{t\tau} \equiv \|\mathbf{t}^0\|_\tau (\xi_{c_\tau} - \xi^0_{c_\tau}) \tag{59}$$

In Eq. (59), $\mathbf{t}^0$ and ξ_c^0 are evaluated at the previous converged load steps and their derivatives can be obtained by taking the variation of the contact consistency condition at load step $n-1$. The material derivative of the tangential slip function in Eq. (59) is

$$\frac{d}{d\tau}(g_t) = v\mathbf{e}_t^T (\mathbf{V} - \mathbf{V}_c + \dot{\mathbf{z}}) + (g_n \|\mathbf{t}^0\|/c)\mathbf{e}_n^T \mathbf{V}_{c,\xi} + \frac{\beta^0 g_t - \|\mathbf{t}^0\|^2}{c^0} \mathbf{e}_t^{0T} (\mathbf{V} - \mathbf{V}_c + \dot{\mathbf{z}}^0) + \frac{g_n^0 \beta^0 (\xi_c - \xi_c^0) - g_n^0 \|\mathbf{t}^0\|}{c^0} \mathbf{e}_n^{0T} \mathbf{V}_{c,\xi} + (\xi_c - \xi_c^0)\mathbf{e}_t^{0T} \mathbf{V}_{c,\xi} \tag{60}$$

where $\dot{\mathbf{z}}^0$ is the material derivative of the displacement at load step $n-1$. Thus the derivative of the tangential slip function at load step n depends on the derivative of the displacement at load step $n-1$ which makes the problem path dependent. For the material derivative of the tangential slip form, the stick and slip conditions are considered separately.

4.2 Design sensitivity formulation for stick condition

The tangential stick form at the perturbed configuration is

$$b_{T\tau}(\mathbf{z}_\tau, \bar{\mathbf{z}}_\tau) = \omega_t \int_{\Gamma_{c\tau}} v_\tau g_{t\tau} \bar{\mathbf{z}}^T \mathbf{e}_{t\tau} \, d\Gamma_\tau \tag{61}$$

and its derivative with respect to the shape design is

$$\frac{d}{d\tau}[b_{T\tau}(\mathbf{z}_\tau, \bar{\mathbf{z}}_\tau)]_{\tau=0} = b_T^*(\mathbf{z}; \dot{\mathbf{z}}, \bar{\mathbf{z}}) + b'_\tau(\mathbf{z}, \bar{\mathbf{z}}) \tag{62}$$

where $b_T^*(\mathbf{z}; \dot{\mathbf{z}}, \bar{\mathbf{z}})$ is same as the tangential stick bilinear form in Eq. (36), by replacing $\Delta\mathbf{z}$ with $\dot{\mathbf{z}}$. In Eq. (62) $b'_T(\mathbf{z}, \bar{\mathbf{z}})$ is a tangential stick fictitious load and is defined by

$$b'_\tau(\mathbf{z},\bar{\mathbf{z}}) = b^*_{\mathrm{T}}(\mathbf{z};\mathbf{V},\bar{\mathbf{z}}) + \omega_{\mathrm{t}}\int_{\Gamma_{\mathrm{c}}}\{(2g_{\mathrm{t}}\|\mathbf{t}\|/c)\bar{\mathbf{z}}^{\mathrm{T}}\mathbf{e}_{\mathrm{t}}\mathbf{e}_{\mathrm{t}}^{0\,\mathrm{T}}\mathbf{V}_{\mathrm{c},\xi} + (2v\beta^0 g_{\mathrm{t}} - v\|\mathbf{t}^0\|^2)\bar{\mathbf{z}}^{\mathrm{T}}\mathbf{e}_{\mathrm{t}}\mathbf{e}_{\mathrm{t}}^{0\,\mathrm{T}}(\mathbf{V}-\mathbf{V}_{\mathrm{c}}+\dot{\mathbf{z}}^0) + (\beta^0 g_{\mathrm{n}}g_{\mathrm{t}}(\|\mathbf{t}\|+\|\mathbf{t}^0\|)/cc^0)\bar{\mathbf{z}}^{\mathrm{T}}\mathbf{e}_{\mathrm{t}}\mathbf{e}_{\mathrm{n}}^{0\,\mathrm{T}}\mathbf{V}_{\mathrm{c},\xi} - (g_{\mathrm{n}}\|\mathbf{t}\|\|\mathbf{t}^0\|^2/cc^0)\bar{\mathbf{z}}^{\mathrm{T}}\mathbf{e}_{\mathrm{t}}\mathbf{e}_{\mathrm{n}}^{0\,\mathrm{T}}\mathbf{V}_{\mathrm{c},\xi} + \kappa v g_{\mathrm{t}}\bar{\mathbf{z}}^{\mathrm{T}}\mathbf{e}_{\mathrm{t}}(\mathbf{V}^{\mathrm{T}}\mathbf{n})\}\mathrm{d}\Gamma \tag{63}$$

Even though the stick condition is considered as a conservative condition, the fictitious load in Eq. (63) depends on the material derivative of the displacement at the previous load step.

4.3
Design sensitivity formulation for slip condition

The tangential slip form at the perturbed configuration is

$$b_{\mathrm{T}\tau}(\mathbf{z}_\tau,\bar{\mathbf{z}}_\tau) = \omega_{\mathrm{t}}\int_{\Gamma_{\mathrm{c}\tau}} v_\tau g_{\mathrm{n}_\tau}\bar{\mathbf{z}}_\tau^{\mathrm{T}}\mathbf{e}_{\mathrm{t}\tau}\,\mathrm{d}\Gamma_\tau \tag{64}$$

where ω_{t} must satisfy the relation in Eq. (39) for the slip condition. The material derivative of Eq. (64) can be taken using the similar procedure as in the stick condition, except the normal gap function, as

$$\frac{\mathrm{d}}{\mathrm{d}\tau}[b_{\mathrm{T}\tau}(\mathbf{z}_\tau,\bar{\mathbf{z}}_\tau)]_{\tau=0} = b^*_{\mathrm{T}}(\mathbf{z};\dot{\mathbf{z}},\bar{\mathbf{z}}) + b'_{\mathrm{T}}(\mathbf{z},\bar{\mathbf{z}}) \tag{65}$$

where $b^*_{\mathrm{T}}(\mathbf{z};\dot{\mathbf{z}},\bar{\mathbf{z}})$ is obtained from the tangential slip bilinear form in Eq. (46) by replacing $\Delta\mathbf{z}$ with $\dot{\mathbf{z}}$. In Eq. (65) $b'_{\mathrm{T}}(\mathbf{z},\bar{\mathbf{z}})$ is a tangential slip fictitious load and is defined by

$$b'_{\mathrm{T}}(\mathbf{z},\bar{\mathbf{z}}) \equiv b^*_{\mathrm{T}}(\mathbf{z};\mathbf{V},\bar{\mathbf{z}}) + \omega_{\mathrm{t}}\int_{\Gamma_{\mathrm{c}}}\{(g_{\mathrm{n}}\|\mathbf{t}\|/c)\bar{\mathbf{z}}^{\mathrm{T}}\mathbf{e}_{\mathrm{t}}\mathbf{e}'^{\,0\,\mathrm{T}}_{\mathrm{t}}\mathbf{V}_{\mathrm{c},\xi} + (v\beta^0 g_{\mathrm{n}}/c^0)\bar{\mathbf{z}}^{\mathrm{T}}\mathbf{e}_{\mathrm{t}}\mathbf{e}_{\mathrm{t}}^{0\,\mathrm{T}}(\mathbf{V}-\mathbf{V}_{\mathrm{c}}+\dot{\mathbf{z}}^0) + (\beta^0 g_{\mathrm{n}}g_{\mathrm{n}}^0\|\mathbf{t}^0\|/cc^0)\bar{\mathbf{z}}^{\mathrm{T}}\mathbf{e}_{\mathrm{t}}\mathbf{e}_{\mathrm{t}}^{0\,\mathrm{T}}\mathbf{V}_{\mathrm{c},\xi} + \kappa v g_{\mathrm{n}}\bar{\mathbf{z}}^{\mathrm{T}}\mathbf{e}_{\mathrm{t}}(\mathbf{V}^{\mathrm{T}}\mathbf{n})\}\mathrm{d}\Gamma \tag{66}$$

Note that the same symbol of $b'_{\mathrm{T}}(\mathbf{z},\bar{\mathbf{z}})$ is used for stick and slip conditions. Thus, the material derivative of the contact variational form can be obtained by combining Eqs. (58) and (63) for the stick condition or Eq. (66) for the slip condition,

$$\frac{\mathrm{d}}{\mathrm{d}\tau}\left[b_{0_{\Gamma_\tau}}(\mathbf{z}_\tau,\bar{\mathbf{z}}_\tau)\right]_{\tau=0} = b^*(\mathbf{z};\dot{\mathbf{z}},\bar{\mathbf{z}}) + b'_{\mathrm{V}}(\mathbf{z},\bar{\mathbf{z}}) \tag{67}$$

where

$$b^*(\mathbf{z};\dot{\mathbf{z}},\bar{\mathbf{z}}) = b^*_{\mathrm{N}}(\mathbf{z};\dot{\mathbf{z}},\bar{\mathbf{z}}) + b^*_{\mathrm{T}}(\mathbf{z};\dot{\mathbf{z}},\bar{\mathbf{z}}) \tag{68}$$

$$b'_{\mathrm{V}}(\mathbf{z},\bar{\mathbf{z}}) = b'_{\mathrm{N}}(\mathbf{z},\bar{\mathbf{z}}) + b'_{\mathrm{T}}(\mathbf{z},\bar{\mathbf{z}}) \tag{69}$$

Thus, if all the terms regarding the material derivative of variational Eq. (45) is collected, then the following system of linear equations can be obtained

$$a^*(\mathbf{z};\dot{\mathbf{z}},\bar{\mathbf{z}}) + b^*(\mathbf{z};\dot{\mathbf{z}},\bar{\mathbf{z}}) = \ell'(\bar{\mathbf{z}}) - a'_{\mathrm{V}}(\mathbf{z},\bar{\mathbf{z}}) - b'_{\mathrm{V}}(\mathbf{z},\bar{\mathbf{z}}), \quad \forall\,\bar{\mathbf{z}}\in\mathbf{Z} \tag{70}$$

The left side of Eq. (70) is of the same form as Eq. (44). Thus, the same decomposed stiffness matrix can be used for analysis and for computing the material derivative of the displacement with the fictitious load. Since the tangent stiffness operator in Eq. (44) is not symmetric, the direct differentiation method is used here. Note that the tangential slip fictitious load depends on the material derivative of the previous converged configuration, Eq. (70) is solved at each load step. Equation (70) is a linear system of equations. Sensitivity computation does not require convergence iterations; only the stiffness matrix at the converged configuration of each load step is used for sensitivity analysis. Since the contact variational term is independent of structural terms in the sensitivity equation, other types of material model can be treated using Eq. (70) if appropriate material derivatives of the structure and load forms are used.

5
Numerical example

Door seals are commonly used for noise isolation and for sealing purposes. The performance of a door seal is evaluated using the contact pressure distribution and the size of contact area. The door is modeled by a rigid body, based on the assumption that the stiffness of the door is much larger compared to that of rubber sealing material.

Figure 3 shows the geometry of the door seal and a portion of the door with discrete particles of RKPM. The geometry of the seal is approximated by a circular shape with the constant thickness except for the mounting part. Only the contact region of the door is modeled for simplicity using a quarter circular section with a 4 mm radius. The geometry of the seal is discretized by 174 particles, and the rigid surface is modeled by 32 piecewise linear master segments. The Mooney-Rivlin type hyper-elastic material is used with a pressure projection formulation [32] for nearly incompressibility constraints. Material constants $C_{10} = 80$ kPa, $C_{01} = 20$ kPa and bulk modulus $K = 80$ MPa are used. The rigid door is pushed down 10 mm from the top of the rubber. The bottom surface of

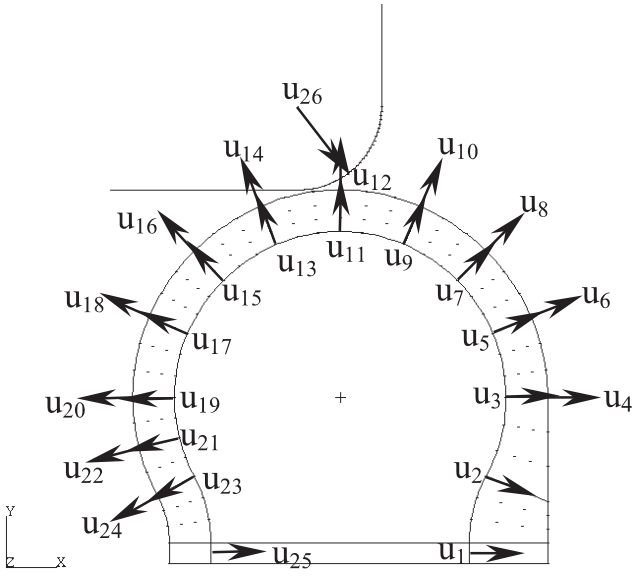

Fig. 3. Design parameters of door seal problem

the door seal refers to the interface of installation and is completely fixed. A flexible-rigid body contact condition is imposed between interfaces. Analysis is carried out with 100 load steps by a displacement driven procedure.

If the friction between the interfaces is ignored, then all the rubber materials are bulged out to the right side without providing effective seal. If friction is considered in this problem, the frictional condition significantly affects the analysis results. A constant value, 0.25, is used as the dry frictional coefficient for all contact surfaces. Figure 4 shows a contour plot of the second invariant of deviatoric Cauchy stress (von Mises stress) with deformed geometry at the final configuration when the friction exists. As the rigid body moves down, the contact region is increased initially. After a certain amount of deformation, the middle part of the contact region starts to separate. Since there is almost no slip between contact surfaces in this problem, all the contact regions are in the stick condition. High stress concentration occurs at the highly distorted region.

The geometry of the structure is parameterized using 26 shape design parameters. The design parameters are shown in Fig. 3. The last design parameter is the radius of the rounded corner of the rigid body. Even though this design parameter does not change the shape of the structure, it can be treated using the material derivative as discussed in Eq. (49). Other 25 design parameters are the parametric coordinate of boundary shapes. The boundaries of the seal are represented by cubic spline curves. The control points or the slopes of the spline curves are chosen as design parameters. The design velocity field at the boundary is obtained first by perturbing the boundary curve corresponding to the design variable and the domain design velocity field is computed using an iso-parametric mapping method [34].

Nine performance measures are chosen: the area of the structure, seven von Mises stresses of the high stress concentrated region, and the square sum of the normal gap distances at the discrete points in the opening region shown in Fig. 4. Note that the stress is proportional to the service life and the normal gap distances are related to the performance of the seal.

DSA is carried out at each converged load step to compute the material derivatives of displacements. Since there are 26 design parameters, 26 linear systems of equations are solved at each load step to compute material derivative of displacements. The sensitivity coefficients of performance measures are computed at the final converged load step using the material derivatives of displacements. The cost of sensitivity computation is about 55% of that of response analysis. Since 26 design parameters are considered in this problem, each design parameter takes less than 3% of analysis computation time. This numerical performance is very efficient compared to that in the finite difference method.

The accuracy of the sensitivity is compared with the forward finite difference results for the perturbation size of $\tau = 10^{-6}$. Table 1 shows accuracy of the sensitivity results. In Table 1, the second column, $\Delta\Psi$, denotes the finite difference results and the third column represents the change of the performance from the proposed method. As can be seen in the table, extremely accurate results are obtained.

The objective of the design problem is to reduce the gap opening by changing the shape of the door seal and the rigid door. The stress concentration is to be reduced at the same time. The area of the rubber components is not so important since the cost of the material is relatively low compared to the other costs. The optimization problem is

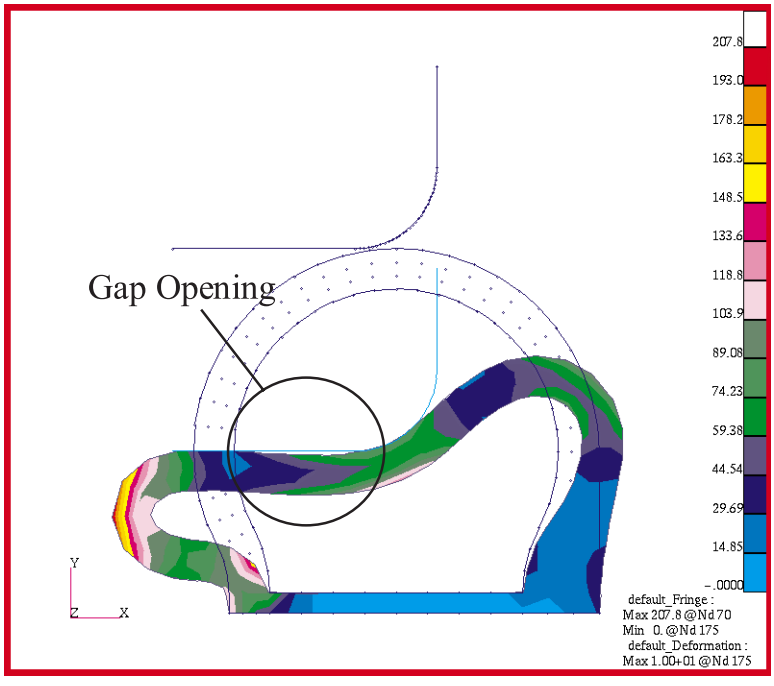

Fig. 4. Stress distribution for door seal problem

Table 1. Accuracy of sensitivity results

Ψ	$\Delta\Psi$	Ψ'	$(\Delta\Psi/\Psi') \times 100$
u_1			
Area	−0.163895E-5	−0.163895E-5	100.00
σ_{75}	−0.501565E-6	−0.501563E-6	100.00
σ_{86}	−0.255777E-5	−0.255775E-5	100.00
σ_{44}	−0.247860E-6	−0.247893E-6	99.99
σ_{114}	0.525571E-6	0.525554E-6	100.00
σ_{31}	−0.149431E-6	−0.149300E-6	100.09
Σg_n^2	−0.114879E-8	−0.114878E-8	100.00
u_2			
Area	0.163894E-5	0.163895E-5	100.00
σ_{75}	0.514388E-6	0.514395E-6	100.00
σ_{86}	−0.268130E-5	−0.268129E-5	100.00
σ_{44}	0.292610E-4	0.292609E-4	100.00
σ_{114}	0.126237E-4	0.126237E-4	100.00
σ_{31}	0.947482E-6	0.947679E-6	99.98
Σg_n^2	0.223116E-7	0.223116E-7	100.00
u_3			
Area	−0.405671E-5	−0.405671E-5	100.00
σ_{75}	−0.858554E-7	−0.858371E-7	100.02
σ_{86}	−0.361270E-5	−0.361266E-5	100.00
σ_{44}	−0.481447E-6	−0.481452E-6	100.00
σ_{114}	0.143501E-5	0.143499E-5	100.00
σ_{31}	0.869462E-7	0.868284E-7	100.14
Σg_n^2	−0.311421E-9	−0.311370E-9	100.02
u_4			
Area	−0.351300E-5	−0.351300E-5	100.00
σ_{75}	−0.105863E-4	−0.105864E-4	100.00
σ_{86}	−0.130646E-4	−0.130647E-4	100.00
σ_{44}	0.122614E-5	0.122615E-5	100.00
σ_{114}	−0.329776E-5	−0.329777E-5	100.00
σ_{31}	−0.243310E-6	−0.243378E-6	99.97
Σg_n^2	−0.210381E-8	−0.210383E-8	100.00
u_5			
Area	0.447486E-5	0.447486E-5	100.00
σ_{75}	0.629273E-5	0.629276E-5	100.00
σ_{86}	0.835460E-5	0.835467E-5	100.00
σ_{44}	0.122614E-5	0.122615E-5	100.00
σ_{114}	0.143353E-5	0.143352E-5	100.00
σ_{31}	0.116624E-6	0.116676E-6	99.96
Σg_n^2	−0.430791E-9	−0.430725E-9	100.02

$$
\begin{aligned}
&\min \sum g_n^2 \\
&\text{s.t. } \text{Area}(109) \le 110 \\
&\quad \sigma_{75}(130) \le 100 \\
&\quad \sigma_{86}(129) \le 100 \\
&\quad \sigma_{44}(209) \le 160 \\
&\quad \sigma_{114}(207) \le 160 \\
&\quad \sigma_{31}(98) \le 100 \\
&\quad \sigma_{38}(191) \le 160 \\
&\quad \sigma_{115}(148) \le 160 \\
&\quad -0.5 \le u_i \le 0.5 \quad i = 0, 26
\end{aligned} \tag{71}
$$

where the values within the parenthesis are original response values. The square sum of the normal gap distances g_n is minimized subjected to reducing selected stresses up to 20% from the initial values and maintaining the rubber area. Since the design parameters are the control points of the geometric curve, the initial values do not have any significant meanings and thus, start from zero initial guesses. The design optimization is carried out using the sequential quadratic programming method (SQP) of the commercial optimization code DOT [35]. The performance values are provided to DOT by solving nonlinear analysis (RKPM) and the sensitivity coefficients are obtained using the proposed method. The initial design is infeasible with all the constraints violated. Optimization is converged after 7 iterations and all the constraints are satisfied. The cost function is reduced to 0.75% of the original value, which is significant reduction considering small changes of design parameters. Even with the impenetration condition slightly violated using the penalty method, all the opened gaps are closed after optimization.

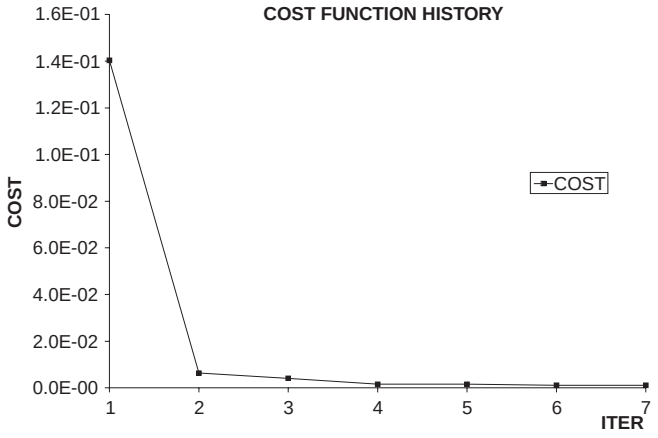

Fig. 5. Cost function (square sum of normal gap distances) history

Figures 5 and 6 show the iteration history of the cost and constraints. In Figure 5, the most significant cost reduction is achieved in first three iterations even though the initial design was infeasible. The constraint violations are adjusted during the last four iterations. Figure 7 shows the results of design optimization. Surprisingly, design parameters are changed only slightly compared to the reduction of the cost and satisfaction of constraint violations. The stress concentrations of the original design are distributed evenly with smaller magnitude, and the contact area is increased significantly.

6 Conclusion

A continuum-based shape design sensitivity formulation for the frictional contact problem with finite deformation in hyper-elastic material is developed. Sensitivity formulation uses the same tangent stiffness matrix as that in the analysis at the converged configuration. No convergence iterations are required for sensitivity computation, and thus sensitivity analysis takes much less effort than nonlinear response analysis. It is also demonstrated that shape optimization of the frictional contact problem can be carried out effectively.

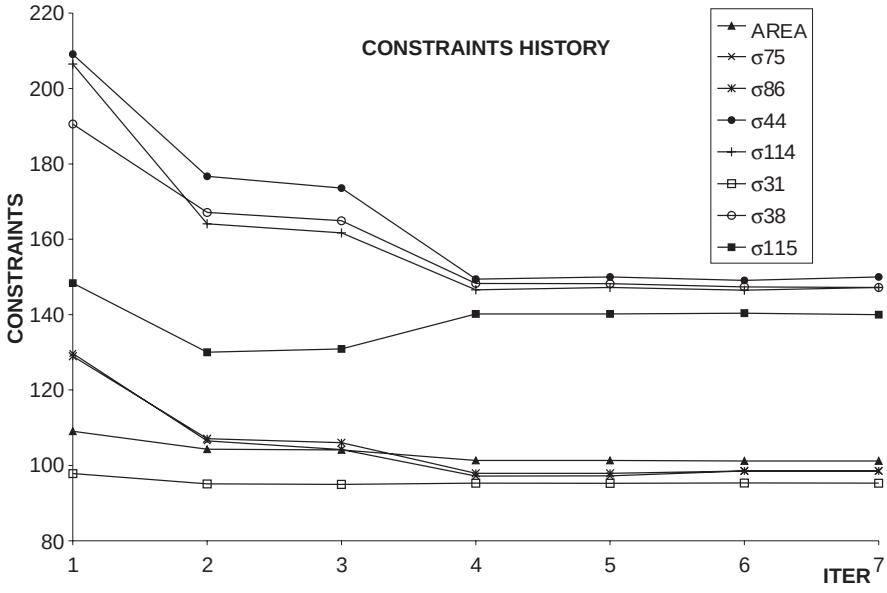

Fig. 6. Constraints function history

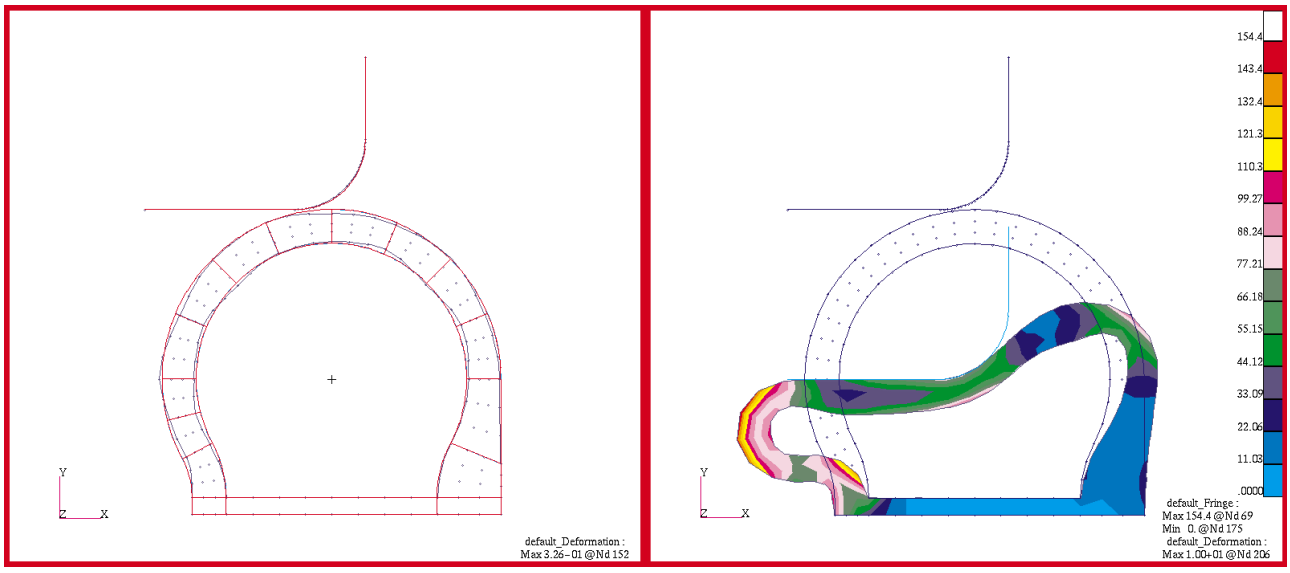

Fig. 7. Optimized shape design and analysis result

References

1. **Stampacchia G, Lions JL** (1965) Inequations Variationnelles Non Coercives. C.R. Acad. Sci., Paris, 261:25–27
2. **Stampacchia G, Lions JL** (1967) Variational inequalities. Com. Pure & Appl. Math. 20:493–519
3. **Hughes TJR, Taylor RL, Sackman JL, Curnier A, Kanoknukulchai W** (1976) A finite element method for a class of contact-impact problems. Comput. Meth. Appl. Mech. Eng. 8:249–276
4. **Kikuchi N, Oden JT** (1988) Contact Problems in Elasticity: A Study of Variational Inequalities and Finite Element Method, SIAM, Philadelphia, PA
5. **Wriggers P, Simo JC** (1985) A note on tangent stiffness for fully nonlinear contact problems. Comp. Appl. Num. Meth. 1:199–205
6. **Parisch H** (1989) A consistent tangent stiffness matrix for three-dimensional nonlinear contact analysis. Int. J. Num. Meth. Eng. 28:1803–1812
7. **Saleeb AF, Chen K, Chang TYP** (1994) An effective two-dimensional frictional contact model for arbitrary curved geometry. Int. J. Num. Meth. Eng. 37:1297–1321
8. **Laursen TA, Simo JC** (1993) A continuum-based finite element formulation for the implicit solution of multibody, large deformation frictional contact problems. Int. J. Num. Meth. Eng. 36:2451–3485
9. **Oden JT, Martins JAC** (1985) Models and computational methods for dynamic frictional phenomena. Comput. Meth. Appl. Mech. Eng. 52:527–634
10. **Michalowski P, Mroz Z** (1978) Associated and non-associated sliding rule in contact friction problems. Arch. Mech. 30:259–276
11. **Wriggers P, Vu Van T, Stein E** (1990) Finite element formulation of large deformation impact-contact problems with friction. Computers and Structures 37:319–331
12. **Mignot F** (1976) Controle dans les Inequations Variationelles Elliptiques. J. Func. Anal. 22:130–185

13. **Sokolowski J, Zolesio JP** (1991) Introduction to Shape Optimization, Springer-Verlag, Berlin
14. **Spivey CO, Tortorelli DA** (1994) Tangent operators, sensitivity expressions, and optimal design of nonlinear elastica in contact with applications to beams. Int. J. Num. Meth. Eng. 37:49–73
15. **Antunez HJ, Kleiber M** (1996) Sensitivity analysis of metal forming process involving frictional contact in steady state. Materials Proc. Tech. 60:485–491
16. **Pollock GD, Noor AK** (1996) Sensitivity analysis of the contact/impact response of composite structures. Comp. Struc. 61:251–269
17. **Santos JLT, Choi KK** (1992) Shape design sensitivity analysis of nonlinear structural systems. Struc. Optim. 4:23–35
18. **Park YH, Choi KK** (1996) Configuration design sensitivity analysis of nonlinear structural systems with elastic material. Mechanics of Structures and Machines 24:217–256
19. **Choi KK, Duan W** (1999) Shape design optimization of nonlinear structures with hyper-elastic materials. Int. J. Num. Meth. Eng., to appear
20. **Lancaster P, Salkauskas K** (1981) Surface generated by moving least squares methods. Math. Comp. 37:141–158
21. **Belytschko T, Lu YY, Gu L** (1994) Element free Galerkin method. Int. J. Num. Meth. Eng. 37:229–256
22. **Liu WK, Jun S, Zhang YF** (1995) Reproducing kernel particle methods. Int. J. Num. Meth. in Fluids 20:1081–1106
23. **Liu WK, Jun S, Li S, Adee J, Belytschko T** (1995) Reproducing kernel particle method for structural dynamics. Int. J. Num. Meth. Eng. 38:1655–1679
24. **Chen JS, Pan C, Wu CT** (1995) Large deformation analysis of rubber based on reproducing kernel particle method. Comp. Mech. 19:153–168
25. **Chen JS, Pan C, Wu CT, Liu WK** (1996) Reproducing kernel particle methods for large deformation analysis of nonlinear structures. Comput. Meth. Appl. Mech. Eng. 139:195–228
26. **Chen JS, Pan C, Roque CMDL, Wang H-P** (1998) A Lagrangian reproducing kernel particle method for metal forming analysis. Comp. Mech. 22:289–307
27. **Liu WK, Chen Y, Uras RA, Chang CT** (1996) Generalized multiple scale reproducing kernel particle methods. Comput. Meth. Appl. Mech. Eng. 139:91–158
28. **Günther FC, Liu WK** (1998) Implementation of boundary conditions for meshless methods. Comput. Meth. Appl. Mech. Eng. 163:205–230
29. **Chen JS, Wu CT, Pan C** (1996) A pressure projection method for nearly incompressible rubber hyper-elasticity. Part I: Theory and Part II: Application, ASME J. Appl. Mech. 63:862–876
30. **Chang TYP, Saleeb AF, Li G** (1991) Large strain analysis of rubber-like materials based on a perturbed Lagrangian variational principles. Comput. Mech. 8:221–233
31. **Grindeanu I, Chang KH, Choi KK, Chen JS** (1998) Design sensitivity analysis of hyper-elastic structures using a meshless method. AIAA J. 36:618–627
32. **Chen JS, Yoon S, Wang H-P, Liu WK** (1999) An improved reproducing kernel particle method for nearly incompressible finite elasticity. Comput. Meth. Appl. Mech. Eng. (in press)
33. **Haug EJ, Choi KK, Komkov V** (1985) Design Sensitivity Analysis of Structural Systems, Academic press, New York, NY
34. **Choi KK, Chang KH** (1994) A study on the velocity computation for shape design optimization. J. Finite Elem. Anal. Design 15:317–347
35. **Vanderplaats GM** (1997) DOT User's Manual, VMA Corp